DESIGN AND OPTIMIZATION OF A HIGH TEMPERATURE THERMAL ENERGY STORAGE WITH DIRECT ELECTRIC CHARGING AND CONVECTIVE DISCHARGING

Matteo Pecchini[1]*, Sunku Prasad Jenne[2], Jihong Wang[2], Anna Stoppato[1] and Alberto Benato[1]

[1]University of Padua, Department of Industrial Engineering, Padova, Italy

[2]University of Warwick, School of Engineering, Coventry, UK

*Corresponding Author: matteo.pecchini@phd.unipd.it

ABSTRACT

High-temperature thermal energy storage (TES) has been widely used in concentrated solar thermal power generation systems and today it is considered one of the most promising technologies for grid-scale electricity storage. In a conventional TES system, the charging and discharging processes are carried out in an indirect contact heat exchanger, which involves transportation losses. Therefore, a high temperature TES that is charged with high-voltage electrical power and discharged with the working fluid of the power cycle is proposed in the present study. A modular design has been developed, which can be extended to any scale. This involves a set of elements made up of an electric heater surrounded by a matrix of ceramic material, which works as storage medium, and air as working fluid for the discharge. The geometry is optimized to have high energy storage density, high air outlet temperature, and minimum pressure drop. Different cross sections, sizes, and void fractions are investigated. The results showed that the elliptical cross section provides the best performance in terms of pressure drops. Moreover, with the elliptical cross section the heat exchange between air and solid material is 2 times more efficient compared to circular and hexagonal elements. Using smaller electric heaters, but larger in number, improves the air heating rate through the reservoir. Increasing the air velocity by 10 times (from 0.1 to 1 m s^{-1}), the heat exchange decreases by 60 to 70% for all the considered cases. Doubling the void fraction from 0.3 to 0.6 causes a reduction in the air heating rate of 35–50%. According to the boundary conditions, the optimal layout of the TES is 10m × 9.6m × 20m. With an air velocity of 0.3 m s^{-1} and a void fraction of 40%, pressure drop with elliptical elements is 1.8 Pa · m^{-1}. Using magnesium oxide as thermal storage medium, the energy density of the proposed thermal storage design results in 390 kWh_{th} m^{-3}.

1 INTRODUCTION

The increasing share of intermittent renewable energy sources (RES) such as solar and wind, is stressing the necessity to develop storage systems capable of storing large amounts of energy at grid level. Among the on-developing technologies, one of the most promising is the so-called Carnot battery (CB), which consists of storing electricity in the form of thermal energy (Benato and Stoppato, 2019). The increasing share of RES is also forcing some conventional power plants, that were designed to run at constant power, to start-up and shut-down several times, or to run at part-load. In other words, the flexibility of power plants must be improved to meet the requirements of the grid. This can be achieved in conventional fossil fuel power plants by integrating thermal energy storage (TES) (Richter et al., 2019). TES can also be included in compressed air energy storage systems (CAES) to increase power and energy density (Houssainy et al., 2018; Li et al., 2019). Thermal energy storage has always been used for different applications, such as concentrated solar power, buildings' heating, and industrial waste heat recovery (Alva et al., 2018; Sarbu and Sebarchievici, 2018; Zhang et al., 2015). However, in recent years, it has also been studied as a potential solution for power applications (Liang et al., 2022; Paul et al., 2022; Richter et al., 2019). Carnot batteries (CB) are one of the most promising TES technologies

https://doi.org/10.52202/077185-0099

for high temperature applications. The CB stores electricity in the form of thermal energy. The scope of this work is the design, optimization, and material selection of a high-temperature thermal energy storage for power applications.

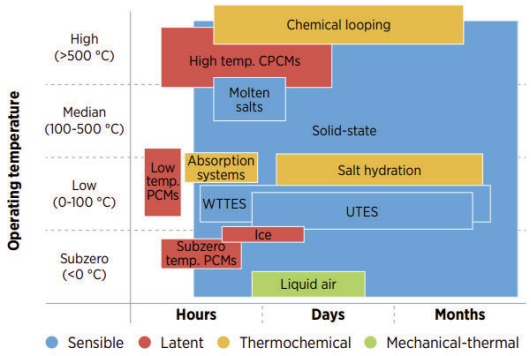

Figure 1: Operating temperatures and time ranges for different TES technologies (Agency (IRENA), 2020).

Thermal storage can be based on sensible heat (in solid or liquid materials), latent heat (using phase change materials), or thermochemical reactions (Liang et al., 2022). The operating temperatures and storage duration for different storage technologies are summarized in Figure 1. Sensible heat storage is the most mature technology, and it is currently used in commercial applications because of its low cost and long lifetime. Moreover, sensible TES can reach high temperatures up to 1400 °C. Typical solid materials suitable for sensible heat storage are cast iron, quartz, graphite, basalt, sand, and ceramic materials like alumina, magnesia and magnetite. These materials can work above 1000 °C (Forsberg et al., 2019; Khare et al., 2013; Liang et al., 2022; Zhao et al., 2022). On the other hand, liquid storage media such as water, sodium, lithium, molten salts, and thermal oils are also used as promising sensible heat storage media but their operating temperature is limited to around 550 °C (Forsberg et al., 2019; Liang et al., 2022; Zhao et al., 2022). Latent thermal energy storage requires smaller volumes, but it has higher costs and a lower maturity compared to sensible storage. Several phase-change materials (PCM) have been studied in literature but, in general, they cannot reach storage temperatures as high as those of ceramic materials (Gil et al., 2010; Liang et al., 2022; Sharma and Mortazavi, 2023). Thermochemical energy storage is the best solution in terms of performance, but costs are very high, and a lot of research still needs to be done to make it competitive on the market (Sunku Prasad et al., 2019).

TES systems are divided in two groups based on the mode of charging, namely external or internal heating (Paul et al., 2022). In external heating systems, the storage media is heated by a heat transfer fluid (HTF) that carries the heat from the source (convective heating). Typical HTFs include, for example, air, carbon dioxide, water, thermal oils, and molten salts (Calderón-Vásquez et al., 2021; Esence et al., 2017). In internal heating systems, the storage medium is heated using electric heaters placed inside the TES (conductive heating) (Stack et al., 2019). Another possibility for internal heating is to apply a potential difference to the storage material and thereby heating it up by Joule heating (Peng et al., 2022). However, for this solution, it is fundamental to use a material that is electrically conductive. Other solutions like volumetric heating (induction, radio frequency, and microwaves heating) have a very low maturity, and very few works were reported in the literature. For both the latter possibilities, it is clear that a suitable TES material that has high storage capacity and the properties for Joule and volumetric heating is seldom present. The discharge phase is usually performed by a convective heat transfer between the heat storage material and HTF to run the power cycle.

A majority of the studies involve a packed-bed configuration for sensible heat storage (Anderson et al., 2014; Calderón-Vásquez et al., 2021; Singh et al., 2010). A packed-bed TES is a cylindrical/rectangular reservoir filled with solid particles of spherical or any random shape. The packed-bed TES is charged with HTF from the top of the tank, and the stored heat is extracted from the packed-bed TES during discharging by passing HTF in reverse direction. Another method of charging/discharging TES system

https://doi.org/10.52202/077185-0099

is creating flow channels in a solid TES matrix (Wu et al., 2014). In this configuration, the HTF is passed through tubes placed inside the solid TES material.
Another possible configuration for solid sensible TES is to arrange the TES material in patterns with provisions for HTF flow. This is similar to packed-bed TES but the storage material is arranged in a structured manner (Wu et al., 2014). Other geometries involve squared channels, honeycomb bricks, ceramic plates, and common bricks (Esence et al., 2019; Kuravi et al., 2013; Stack et al., 2019). Regarding sensible liquid storage, there are two possibilities: the double-tank configuration and the thermocline configuration. The double tank configuration is more expensive, but it does not suffer from thermocline degradation over time (Liang et al., 2022). In general, regarding the shape of the overall TES, rectangular shape is used for sensible storage, while cylindrical shape is preferred for latent thermal energy storage systems (Mao, 2016).
The aim of this work is to develop a TES system for excess renewable energy storage suitable for grid-scale applications. In a conventional TES system, the charging and discharging processes are carried out in an indirect contact heat exchanger, which involves transportation losses. Therefore, a high temperature TES that is charged with high-voltage electrical power and discharged with the working fluid of the power cycle is proposed and studied. With direct electric heating, thermal losses and pressure drop in the HTF flow can be reduced, and it is easier to integrate the system with the RES and connecting to the grid. Therefore, the main objective of the present study is to identify suitable heat storage materials for direct electric heating and to optimize the design of such TES configuration for directly integrating heating elements into it. The potential applications of the present technology are supercritical CO_2 power cycles, compressed air energy storage systems, and Carnot batteries.
In Section 2, the design of the TES, materials selection, and methodology for modeling are described. Section 3 shows the results of optimization, and the choice of the final shape of the TES. The major outcomes of the present study are summarized in Section 4.

2 PHYSICAL SYSTEM AND MATHEMATICAL MODELING

2.1 Design of the TES system

The schematic of the TES system designed for direct heating with embedded electric heaters during charging and convective discharging is shown in Figure 2. Unlike a packed bed TES system, the storage elements are arranged in an array and each storage element is embedded with an electric heater (EH). During discharging, the HTF (i.e., air in the present study) is passed through the array of storage elements to extract the heat and supply it to the power cycle. The shape of the storage elements influences the heat transfer, and the pressure drops through the reservoir. Different cross-sectional shapes of the storage elements such as circular, elliptical, and hexagonal are evaluated. The design variables of the TES are shown in Table 1. The design process consisted of varying these design variables to evaluate the influence on the performance indicators shown in Table 1. The objective is to minimize the pressure drop and maximize the air heating rate. The *air heating rate* (HR) is defined as the temperature rise per unit of storage element.

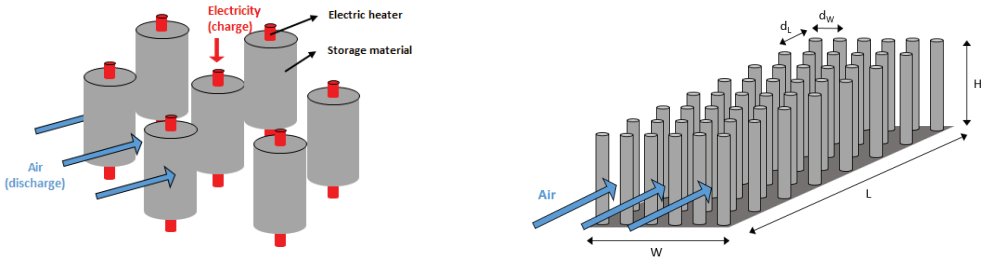

(a) Structure of single storage elements (b) Overall design of the TES

Figure 2: Overview of the setup of the TES.

https://doi.org/10.52202/077185-0099

Table 1: Independent variables and performance indicators for discharge simulations.

Design variables		**Range**
W [m]	TES width	\
L [m]	TES length	\
H [m]	TES height	\
d_W [m]	distance between elements along the width	0.08 – 0.49
d_L [m]	distance between elements along the length	0.15 – 0.54
v_{air} [m/s]	inlet air velocity	0.1 – 1.1
VF [-]	void fraction	0.3 – 0.7
Performance indicators		
HR [°C/element]	air heating rate	
Δp [Pa/element]	pressure losses	

Firstly, the cross-sectional shape of the storage element is optimized during charging. The model was set as shown in Figure 3. A quarter of the cross section was considered by imposing symmetry conditions. The EH was modeled by imposing a specific power on the internal surface of the rod. Having fixed the desired charging time (6 hours), and the initial temperature of the rod (400°C), the charge is considered complete when the average temperature of the storage material reaches the design storage temperature (950°C). In this way it was possible to define the possible cross-sections. Once defined, the elements have been set in a staggered configuration.
The next step consisted of designing the array of storage elements. This is done by analyzing the influence of the design parameters on the performance of the storage system (see Table 1). Parametric studies during discharging were performed for this purpose. As shown in Figure 4, d_W and d_L represent the distance between the elements along the width and along the length, respectively. The storage material is initially set at the design storage temperature of 950°C. The TES is discharged, imposing a flow rate of air through the reservoir. The air is at a lower temperature (400°C) compared to storage media. Therefore, by passing through the TES, the ceramic material releases heat to the air flow. The physical domain considered for the discharge simulation is shown in Figure 4.

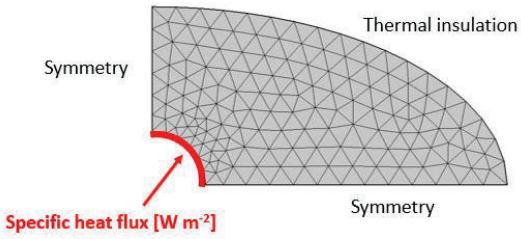

Figure 3: Model set up for the definition of the cross-sectional shape of the storage elements.

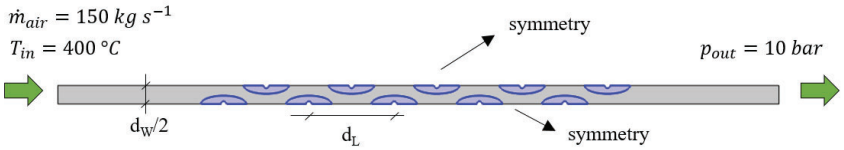

Figure 4: Model set up for the discharge CFD simulations.

2.2 Materials

The electric heaters were selected from the commercial catalog of *Kanthal* company (Kanthal, n.d.). The catalog provides the specific power and the diameter of the heating element. Two different heaters

https://doi.org/10.52202/077185-0099

have been tested: one of 40 kW m^{-2} with a diameter of 5.6 cm (referred as EH1), and the other of 35 kW m^{-2} with a diameter of 2.0 cm (referred as EH2). As explained in Section 3.1, given the same amount of total energy the use of EH2 involves 3.3 times the number of elements compared to the use of EH1. Therefore, to make a consistent comparison (i.e., per unit of energy, in addition to per unit of element) between the different configurations, the performance indicators obtained by the discharge simulations for the cases with EH2 are multiplied by 3.3.

Air is selected as a heat transfer fluid and magnesium oxide (MgO) is selected as the TES because of its thermal stability and because it is inexpensive, and it has good thermal properties. The thermal properties of MgO are shown in Equations 1-3 (Chase, 1998; Green and Perry, 2007; Rao and Narender, 2014). Specific heat is expressed in J $kg^{-1}K^{-1}$, thermal conductivity in W $m^{-1}K^{-1}$, and density in kg m^{-3}. Temperature is expressed in K.

$$cp_{MgO} = 275.07 + 3.35\,T - 4.8448 \cdot 10^{-3}\,T^2 + 3.7854 \cdot 10^{-6}\,T^3 - 1.6246 \cdot 10^{-9}\,T^4 + 3.6106 \cdot 10^{-13}\,T^5 - 3.2416 \cdot 10^{-17}\,T^6 \quad (1)$$

$$\rho_{MgO} = 3.65\,10^3 \exp\left(-3 \cdot 10^{-6}(-3.7483 \cdot 10^3 + 12.5491\,T - 1.3512 \cdot 10^{-5}\,T^2 + 3.0399 \cdot 10^{-7}\,T^3)\right) \quad (2)$$

$$\lambda_{MgO} = 120.8873 - 0.3584\,T + 4.7914 \cdot 10^{-4}\,T^2 - 3.3046 \cdot 10^{-7}\,T^3 + 1.1403 \cdot 10^{-10}\,T^4 - 1.5410 \cdot 10^{-14}\,T^5 \quad (3)$$

2.3 Assumptions

The following assumptions are considered in the modeling.

- The storage material is homogeneous and isotropic.
- Heat losses from the TES are neglected i.e., adiabatic boundary condition.
- The effect of radiation is neglected.
- A safe temperature gradient of 150°C is assumed across the storage element while varying the dimensions of the storage elements to avoid thermal shock and failure.
- The heat capacity of the electric heaters is neglected during charge and discharge.
- For discharge simulations, only a portion of the total width of the TES is considered by imposing symmetry conditions (Bacellar et al., 2016).

2.4 Governing Equations

The governing equations for the charging and discharging process are shown in this Section.

The charging phase consists of heating the TES medium using electric heaters, which does not involve any fluid flow. Hence, the energy equation in solid, as shown in Eq. 4 is used.

$$\frac{\partial(\rho_s cp_s T_s)}{\partial t} - \nabla \cdot (k_s \nabla \cdot T_s) = 0 \quad (4)$$

During discharge, air passes over the TES elements and therefore mass, momentum and energy equations are used for the modeling. Equation 5 represents the continuity equation. Equations 6 and 7 are the momentum equations in the two dimensions, while Equation 8 is the energy equation. In addition, the equation of state relates the density with the pressure and the temperature.

$$\frac{\partial \rho_f}{\partial t} + \nabla \cdot (\rho_f\, u) = 0 \quad (5)$$

$$\frac{\partial(\rho_f u_x)}{\partial t} + \nabla \cdot (\rho_f\, u_x\, u) = -\frac{\partial p}{\partial x} + \nabla \cdot (\mu\, \nabla\, u_x) + S_{M,x} \quad (6)$$

$$\frac{\partial(\rho_f u_y)}{\partial t} + \nabla \cdot (\rho_f\, u_y\, u) = -\frac{\partial p}{\partial y} + \nabla \cdot (\mu\, \nabla\, u_y) + S_{M,y} \quad (7)$$

$$\frac{\partial(\rho_f h_f)}{\partial t} - \frac{\partial p}{\partial t} + \nabla \cdot (\rho_f\, u\, h_f) = \nabla\left[\left(\mu + \frac{\mu_t}{\sigma_t}\right)\nabla h_f\right] - S_h \quad (8)$$

The k-ε turbulence model used for the simulations introduces two additional transport equations (Eq. 9 and Eq. 10) and two dependent variables (the turbulent kinetic energy, k, and the turbulent dissipation rate, ε), which are correlated by the equation $\mu_t = \rho\, C_\mu \frac{k^2}{\epsilon}$.

$$\rho \frac{\partial k}{\partial t} - \rho u \cdot \nabla k = \nabla\left[\left(\mu + \frac{\mu_t}{\sigma_k}\right)\nabla k\right] + S_k - \rho\, \epsilon \quad (9)$$

https://doi.org/10.52202/077185-0099

$$\rho\frac{\partial\epsilon}{\partial t}-\rho\mathbf{u}\cdot\nabla\epsilon=\nabla\left[\left(\mu+\frac{\mu_t}{\sigma_\epsilon}\right)\nabla\epsilon\right]+C_{\epsilon,1}\frac{\epsilon}{k}S_k-C_{\epsilon,2}\rho\frac{\epsilon^2}{k} \quad (10)$$

2.5 Initial and boundary conditions

In the present study, the TES system operates between 400 and 950°C. During charging, the initial temperature of TES is 400°C and is raised to an average temperature of 950°C using electrical heaters. The target charging time for the sizing of the storage elements is 6 hours. During discharge, the initial temperature is set at 950°C while the air is passed through the TES system with an inlet temperature of 400°C, an outlet pressure of 10 bar and a flow rate of 150 kg s^{-1}. The operating conditions for charging and discharging are selected that are suitable for CAES and PTES systems. The boundary conditions for the discharge simulations are shown in Figure 4. For the stability of the simulations the outlet pressure was imposed as boundary condition. The model is set choosing a *weakly compressible* flow, in which the density depends only on the temperature, with a reference pressure set to 10 bar. In this way, the pressure drop is evaluated by as the difference between the inlet pressure (output of the simulation) and the outlet pressure (set as boundary condition).

2.6 Meshing

A mesh-sensitivity analysis was performed to evaluate the number of elements necessary to obtain sufficient accuracy in the results of CFD simulations. The target parameters chosen for these comparisons are the outlet air temperature and the pressure drop across the array. For the mesh sensitivity analysis, an array with 10 rows of elliptic TES elements is used. The inlet air velocity is set to 0.5 m s^{-1}. The number of elements in the mesh was varied to understand the influence on the accuracy of the results (see Figure 5). The temperature evaluation is always very accurate (the error is always below 5% even with the coarsest mesh). On the other hand, the pressure drop displays a not negligible error (> 10%) if the number of elements is less than 3 10^4 every 10 rows of TES elements. However, pressure losses are always within an acceptable range for the considered mesh sizes. Therefore, the mesh density of around 40000 to 60000 elements for every 10 rows of TES elements is chosen for the present study.

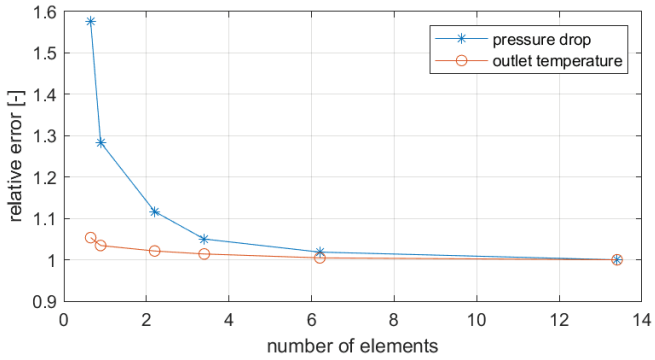

Figure 5: Results of the mesh sensitivity analyses.

3 Results and discussion

For the given storage capacity, the cross section of the storage element, the number of storage elements, and the arrangement of the storage elements play a major role in determining the charging behavior and discharging performance in terms of pressure drops and air outlet temperature. Therefore, the cross section and the geometry of the TES system are studied and optimized for minimum temperature gradient during charging and minimum pressure drop and good efficient air heat exchange during discharging. The charging and discharging results are presented in Section 3.1 and Section 3.2, respectively.

https://doi.org/10.52202/077185-0099

3.1 Cross-section of the storage element

The charging behavior of the storage elements is simulated for the charging duration of 6 hours, the initial temperature of the elements of 400°C and the target final temperature of 950°C. Circular, elliptical, and hexagonal cross sections are studied under two different heat flux boundary conditions. The results of the optimization are shown in Figure 6. Due to the smaller size and power of EH2, the resulting cross-sections are smaller compared to using the bigger and more powerful EH1. For example, the radius of cylindrical elements is 14.2cm for the case with EH1, and 7.7cm for the case with EH2. Therefore, storage elements with EH1 are made up of 3.3 times more storage material than the case with EH2. This means that, given the same total amount of total energy (i.e. same amount storage material), the TES with the smallest electric heaters (EH2) needs 3.3 times more elements than the EH1. As shown later, this will affect heat exchange and pressure drops. Due to asymmetry of the elliptical cross section, there exist infinite possible aspect ratios that can provide a charging time of 6 hours. Therefore, the aspect ratio of the ellipse is selected such that it will satisfy the safe operating temperature gradient limit. A stretched profile leads to lower pressure drops during the discharge. The use of EH2 allows for a more stretched elliptical cross-section shape. With the biggest electric heater, the semiaxis of the elliptical cross-section measures 23.4 and 8.6cm. For the case with the EH2 they measure 22.2 and 2.7cm. The storage elements represented in Figure 6 have been arranged in staggered configurations to find the best design of the overall reservoir.

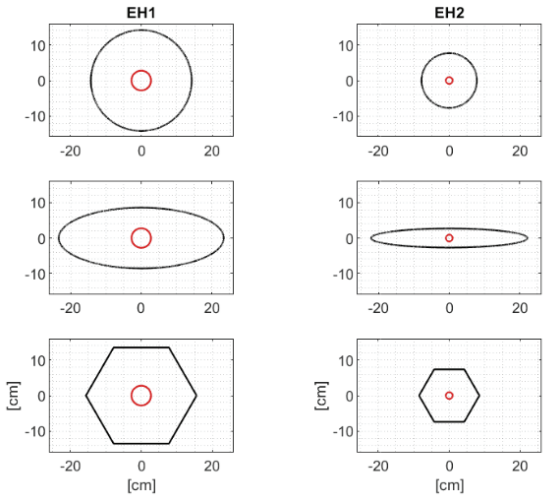

Figure 6: Resulting cross-sectional shapes for the two different electric heaters.

3.2 TES layout optimization

Once the cross section of the TES elements was optimized, the layout of the TES was optimized in terms of aspect ratio of the array and the distance between the elements. Therefore, a thermal-fluid analysis was conducted for the discharge phase. The heating elements are set to the initial temperature of 950°C. The objective is to design a TES with low pressure losses and effective heat exchange. The independent variables that define the TES design, and the performance indicators are summarized in Table 1.

The position of the elements inside the reservoir influences the performance of the storage system. The effect of the variation of d_W and d_L was investigated with parametric simulations. Similarly to what was done for the mesh sensitivity analysis, simulations are performed imposing an air velocity of 0.5 m s^{-1} through 10 rows of cylindrical elements. The results are represented in Figure 7a and Figure 7b. These are expressed in the form of relative variation considering a reference point characterized by d_W = 38.0 cm and d_L = 32.9 cm (VF = 0.5). Figure 7a reveals that d_W is the only parameter that affects the heat exchange, and increasing it by 30% leads to a decrease in the air outlet temperature of approximately 7%. On the other hand, d_L has almost no influence on the heat exchange. Similarly, pressure drops are mainly affected by d_W, while the influence of d_L is weak. Based on these results, the authors decided to

https://doi.org/10.52202/077185-0099

proceed keeping constant the ratio between d_W and d_L; making these two parameters dependents, allowed performing the following simulations using the void fraction (VF) as driving design parameter.

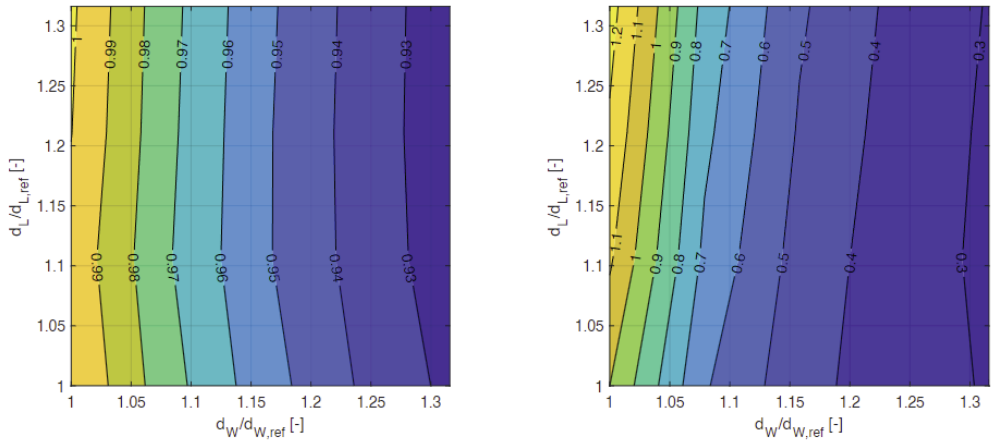

(a) Relative variation of the air heating rate. (b) Relative variation of the pressure drops.

Figure 7: Influence of the distance between elements on the performance of the TES. Variation in air heating rate and pressure drop are relative to the reference case ([1, 1]), which corresponds to a void fraction of 0.5.

Once it was stated that d_W and d_L can be considered substantially as dependent variables, the performance of the system can be analyzed as a function of the void fraction in the TES. Figure 8a and Figure 8b show the influence of VF on the heating rate and pressure drops, respectively. Both decrease with the void fraction. Doubling the VF from 30 to 60%, the air heating rate decreases by 40 to 50% for all the cases under investigation, except for the EH2 with elliptical elements, which decreases by 35%. The air HR is 8 times lower in the case with EH1 compared to the case with EH2 for elliptical shape. In addition, heat exchange is twice as efficient for EH2 with an elliptical shape, compared to the circular and hexagonal shape. This is because the ellipse is highly stretched, and given the same amount of material, a greater heat exchange area improves the air heating rate. The pressure drops for the elliptical bars are slightly lower than those for the circular elements, and significantly lower than those for the hexagonal ones. However, for very low VF values, the pressure drops for the elliptical bars, especially with EH2, suddenly increases because at low porosity the minimum distance between elliptical elements is very low. However, the pressure drop always remains below 70 Pa/element which is considered an acceptable value.

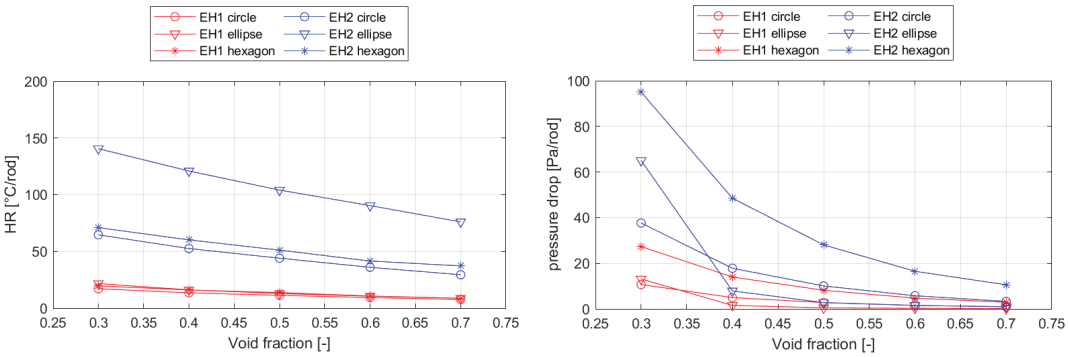

(a) Variation of air heating (HR) with VF. (b) Variation of pressure drops with VF

Figure 8: Influence of the void fraction and cross-sectional shape on the performance of the system. All these simulations are performed with an inlet air velocity of 0.5 m s^{-1}.

https://doi.org/10.52202/077185-0099

The air mass flow rate is given by preliminary studies on power and storage plants. However, by varying the frontal area of the TES (H and W), it is possible to have different inlet air velocities. Therefore, the influence of air velocity on the performance of the storage system is studied in this Section. Figure 9a shows how the air velocity affects the air outlet temperature. Figure 9b shows how pressure drops depend on the air velocity. Circular, elliptical, and hexagonal shapes are tested, and all simulations are performed with the same void fraction (VF = 0.5). The heating rate decreases with the air velocity. Increasing v_{air} by 10 times, the air heating rate decreases by 60 to 70% for all the cases under investigation. The heat exchange is particularly enhanced with the electric heater EH2 and elliptical cross-section. The pressure drops increase with higher air speeds. Circular and hexagonal elements imply losses that are 5–7 and 16–19 times higher than those of the elliptical shape, respectively. From these results, it can be derived that the hexagonal cross-section does not provide a significant improvement in the air heating, while it involves really high pressure losses. Nevertheless, hexagons are geometrically suitable for reaching high compactness (low porosity). However, with void fractions lower than 30%, the fluid flow must be carefully analyzed, as it can be considered more as an internal flow, rather than an external flow.

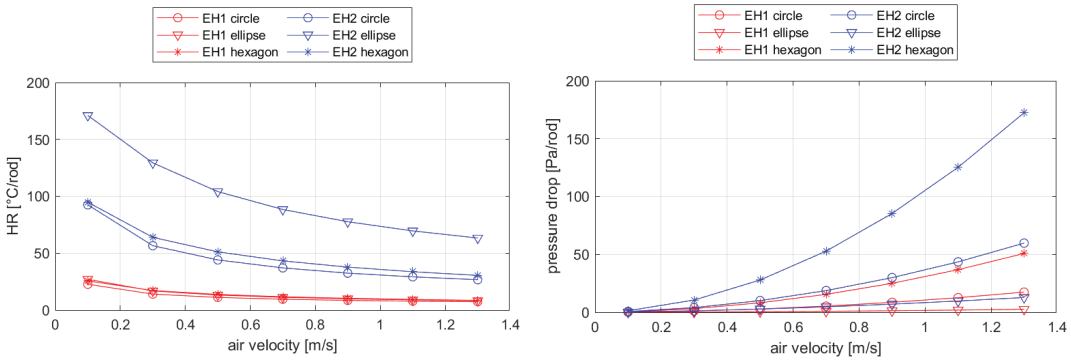

(a) Variation of air heating (HR) with v_{air}. (b) Variation of pressure drops with v_{air}.

Figure 9: Influence of air velocity and cross-sectional shape on the performance of the system. All these simulations are performed with a VF of 0.5.

The analyses described above provided useful guidelines for the design and optimization of a solid sensible TES with direct electrical charging and convective discharging. Parametric simulations have been carried out to study the influence of design variables on the performance of the storage system. The TES has been optimized to maximize heat exchange and minimize pressure drops during discharge. The results showed that a low air velocity is beneficial both for heat exchange and pressure drops, and a low void fraction enhances the heat exchange between air and solid storage material. A low porosity also implies higher pressure losses; however, these remain within the acceptability range. Elliptical and hexagonal cross sections cause the lowest and the highest pressure drops, respectively. The best solution in terms of heat exchange is the electric heater EH2 coupled with an elliptical cross-sectional shape.
Based on all these considerations, the TES was designed with the smallest electric heater (EH2), elliptical cross-sectional shape of the storage elements, and a void fraction of 0.4. Given a total power of the electric heaters equal to 125 MW, the optimal overall TES layout resulted in H=10m, W=9.6m and L=20m (the resulting v_{air} is around 0.3 m s^{-1}). The total pressure drop through the reservoir is 37 Pa (1.9 Pa m^{-1}). With MgO as storage material, the energy storage density results in 390 kWh m^{-3}. For the so-made thermal energy storage, it was simulated a complete discharge, imposing an air mass flow rate of 150 kg s^{-1} with an inlet temperature of 400 °C and an inlet pressure of 10 bar. Figure 10 shows the air temperature profile inside the reservoir. Figure 11 shows the air outlet temperature over time. For the power production application, it is better to have the highest possible air temperature. The systems where this TES is supposed to work (e.g., CAES systems) have a typical discharge interval of 4–8 hours. Within this time range, the air temperature remains always above 600°C.

https://doi.org/10.52202/077185-0099

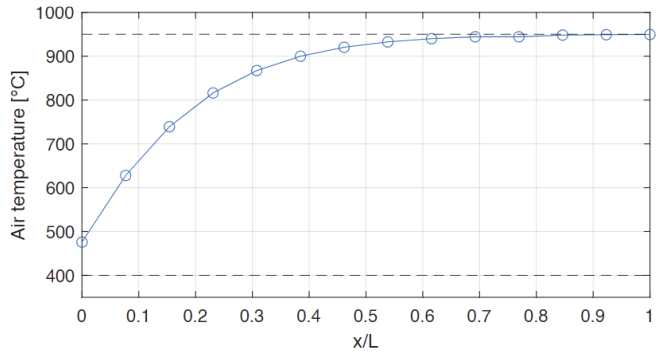

Figure 10: Trend of the air temperature trend inside the TES at the beginning of the discharge.

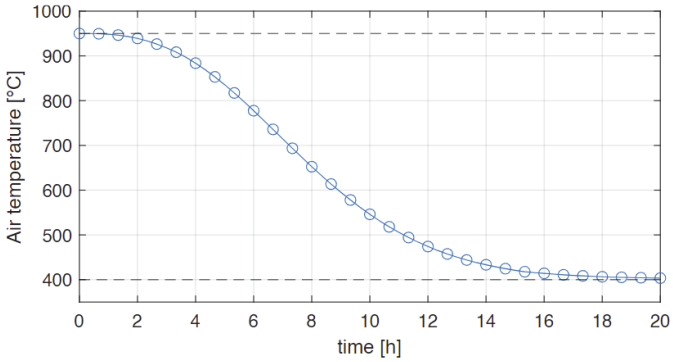

Figure 11: Air outlet temperature over time for a full discharge process.

4 CONCLUSIONS

The design of a sensible solid thermal energy storage with direct electrical charging and convective discharging has been carried out in this work. The TES is designed considering a set of storage elements made up of an electric heater surrounded by ceramic material. Given a total electrical power of 125 MW_{el} (750 MWh_{th} of capacity) the optimal TES layout was found with H=10m, W=9.6m and L=20m. This allows to have a low inlet air velocity (0.3 m s^{-1}). Setting a void fraction of 0.4 represents the best trade-off between heat exchange and pressure drops. Using smaller electric heaters, but larger in number, improves the air heating rate through the reservoir. The results showed that an elliptical cross-section of the storage elements allowed low pressure drops (less than 2 Pa m^{-1}) and a heat exchange 2 times higher compared to circular and hexagonal elements.
Future investigations should involve 3D simulations to evaluate the influence of the walls. Different storage materials can be compared to magnesium oxide. Finally, the results of CFD simulations can be compared to 1D mathematical models from the literature.

NOMENCLATURE

Abbreviations

CAES	Compressed Air Energy Storage
CB	Carnot Battery
EH	Electric Heater
HTF	Heat Transfer Fluid
RES	Renewable Energy Sources
TES	Thermal Energy Storage
VF	Void Fraction

https://doi.org/10.52202/077185-0099

Constants and variables

T	temperature (°C)
p	pressure (bar)
HR	heating rate (°C rod^{-1})
$\dot{m}$	mass flow rate (kg s^{-1})
cp	specific heat (J $kg^{-1}K^{-1}$)
λ	thermal conductivity (W m^{-1} K^{-1})
v	velocity (m s^{-1})

Subscripts and superscripts

in	inlet
out	outlet
el	electrical
th	thermal

REFERENCES

Agency (IRENA), I.R.E. (Ed.), 2020. Innovation Outlook: Thermal Energy Storage. Abu Dhabi.

Alva, G., Lin, Y., Fang, G., 2018. An overview of thermal energy storage systems. Energy 144, 341–378. doi:10.1016/J.ENERGY.2017.12.037

Anderson, R., Shiri, S., Bindra, H., Morris, J.F., 2014. Experimental results and modeling of energy storage and recovery in a packed bed of alumina particles. Appl. Energy 119, 521–529. doi:10.1016/J.APENERGY.2014.01.030

Bacellar, D., Aute, V., Huang, Z., Radermacher, R., 2016. Airside friction and heat transfer characteristics for staggered tube bundle in crossflow configuration with diameters from 0.5mm to 2.0mm. Int. J. Heat Mass Transf. 98, 448–454. doi:https://doi.org/10.1016/j.ijheatmasstransfer.2016.02.072

Benato, A., Stoppato, A., 2019. Integrated Thermal Electricity Storage System: Energetic and cost performance. Energy Convers. Manag. 197. doi:10.1016/j.enconman.2019.111833

Calderón-Vásquez, I., Cortés, E., García, J., Segovia, V., Caroca, A., Sarmiento, C., Barraza, R., Cardemil, J.M., 2021. Review on modeling approaches for packed-bed thermal storage systems. Renew. Sustain. Energy Rev. 143. doi:10.1016/j.rser.2021.110902

Chase, M., 1998. NIST-JANAF Thermochemical Tables, 4th Edition. American Institute of Physics, -1.

Esence, T., Bruch, A., Molina, S., Stutz, B., Fourmigué, J.-F., 2017. A review on experience feedback and numerical modeling of packed-bed thermal energy storage systems. Sol. Energy 153, 628–654. doi:10.1016/j.solener.2017.03.032

Esence, T., Desrues, T., Fourmigué, J.-F., Cwicklinski, G., Bruch, A., Stutz, B., 2019. Experimental study and numerical modelling of high temperature gas/solid packed-bed heat storage systems. Energy 180, 61–78.

Forsberg, C., Sabharwall, P., Gougar, H.D., n.d. Heat Storage Coupled to Generation IV Reactors for Variable Electricity from Base-load Reactors: Workshop Proceedings: Changing Markets, Technology, Nuclear-Renewables Integration and Synergisms with Solar Thermal Power Systems.

Gil, A., Medrano, M., Martorell, I., Lázaro, A., Dolado, P., Zalba, B., Cabeza, L.F., 2010. State of the art on high temperature thermal energy storage for power generation. Part 1-Concepts, materials and modellization. Renew. Sustain. Energy Rev. 14 1 , 31–55. doi:10.1016/J.RSER.2009.07.035

Green, D.W., Perry, R.H., 2007. Perry's Chemical Engineers' Handbook, Eighth Edition, McGraw Hill professional. McGraw Hill LLC.

Houssainy, S., Janbozorgi, M., Ip, P., Kavehpour, P., 2018. Thermodynamic analysis of a high temperature hybrid compressed air energy storage (HTH-CAES) system. Renew. Energy 115, 1043–1054. doi:10.1016/j.renene.2017.09.038

https://doi.org/10.52202/077185-0099

Kanthal (Ed.), n.d. Resistance heating alloys and systems for industrial furnace.
Khare, S., Dell'amico, M., Knight, C., Mcgarry, S., 2013. Selection of materials for high temperature sensible energy storage. doi:10.1016/j.solmat.2013.03.009
Kuravi, S., Trahan, J., Goswami, Y., Jotshi, C., Stefanakos, E., Goel, N., 2013. Investigation of a high-temperature packed-bed sensible heat thermal energy storage system with large-sized elements. J. Sol. Energy Eng. Trans. ASME 135 4 . doi:10.1115/1.4023969
Li, Y., Miao, S., Yin, B., Yang, W., Zhang, S., Luo, X., Wang, J., 2019. A real-time dispatch model of CAES with considering the part-load characteristics and the power regulation uncertainty. Int. J. Electr. Power Energy Syst. 105, 179–190. doi:10.1016/j.ijepes.2018.08.024
Liang, T., Vecchi, A., Knobloch, K., Sciacovelli, A., Engelbrecht, K., Li, Y., Ding, Y., 2022. Key components for Carnot Battery: Technology review, technical barriers and selection criteria. Renew. Sustain. Energy Rev. 163, 112478. doi:10.1016/J.RSER.2022.112478
Mao, Q., 2016. Recent developments in geometrical configurations of thermal energy storage for concentrating solar power plant. Renew. Sustain. Energy Rev. 59, 320–327.
Paul, A., Holy, F., Textor, M., Lechner, S., 2022. High temperature sensible thermal energy storage as a crucial element of Carnot Batteries: Overall classification and technical review based on parameters and key figures. J. Energy Storage 56. doi:10.1016/j.est.2022.106015
Peng, P., Yang, L., Menon, A., Weger, N., Prasher, R., Breunig, H., Lubner, S., 2022. Techno-economic Analysis of High-Temperature Thermal Energy Storage for On-Demand Heat and Power.
Rao, A., Narender, K., 2014. Studies on thermophysical properties of CaO and MgO by-ray attenuation. J. Thermodyn. 2014.
Richter, M., Oeljeklaus, G., Görner, K., 2019. Improving the load flexibility of coal-fired power plants by the integration of a thermal energy storage. Appl. Energy 236, 607–621.
Sarbu, I., Sebarchievici, C., 2018. A comprehensive review of thermal energy storage. Sustain. Switz. 10 1 . doi:10.3390/su10010191
Sharma, S., Mortazavi, M., 2023. Pumped thermal energy storage: A review. Int. J. Heat Mass Transf. 213, 124286. doi:10.1016/j.ijheatmasstransfer.2023.124286
Singh, H., Saini, R.P., Saini, J.S., 2010. A review on packed bed solar energy storage systems. Renew. Sustain. Energy Rev. 14 3 , 1059–1069. doi:10.1016/J.RSER.2009.10.022
Stack, D.C., Curtis, D., Forsberg, C., 2019. Performance of firebrick resistance-heated energy storage for industrial heat applications and round-trip electricity storage. Appl. Energy 242, 782–796. doi:10.1016/j.apenergy.2019.03.100
Sunku Prasad, J., Muthukumar, P., Desai, F., Basu, D.N., Rahman, M.M., 2019. A critical review of high-temperature reversible thermochemical energy storage systems. Appl. Energy 254, 113733. doi:10.1016/j.apenergy.2019.113733
Wu, M., Li, M., Xu, C., He, Y., Tao, W., 2014. The impact of concrete structure on the thermal performance of the dual-media thermocline thermal storage tank using concrete as the solid medium. Appl. Energy 113, 1363–1371. doi:10.1016/J.APENERGY.2013.08.044
Zhang, H., Baeyens, J., Cáceres, G., Degrève, J., Lv, Y., 2015. Thermal energy storage: Recent developments and practical aspects. Prog. Energy Combust. Sci. 53, 1–40. doi:10.1016/j.pecs.2015.10.003
Zhao, Yongliang, Song, J., Liu, M., Zhao, Yao, Olympios, A.V., Sapin, P., Yan, J., Markides, C.N., 2022. Thermo-economic assessments of pumped-thermal electricity storage systems employing sensible heat storage materials. Renew. Energy 186, 431–456. doi:10.1016/J.RENENE.2022.01.017

ACKNOWLEDGEMENT

The authors would like to thank EPSRC Hi-CAES project (EP/W027372/1) funding support.

https://doi.org/10.52202/077185-0099